Simulating the global distribution of nitrogen isotopes in the ocean

Christopher J. Somes,[1] Andreas Schmittner,[1] Eric D. Galbraith,[2] Moritz F. Lehmann,[3] Mark A. Altabet,[4] Joseph P. Montoya,[5] Ricardo M. Letelier,[1] Alan C. Mix,[1] Annie Bourbonnais,[6] and Michael Eby[6]

Received 13 January 2010; revised 21 June 2010; accepted 21 July 2010; published 30 November 2010.

[1] We present a new nitrogen isotope model incorporated into the three-dimensional ocean component of a global Earth system climate model designed for millennial timescale simulations. The model includes prognostic tracers for the two stable nitrogen isotopes, ^{14}N and ^{15}N, in the nitrate (NO_3^-), phytoplankton, zooplankton, and detritus variables of the marine ecosystem model. The isotope effects of algal NO_3^- uptake, nitrogen fixation, water column denitrification, and zooplankton excretion are considered as well as the removal of NO_3^- by sedimentary denitrification. A global database of $\delta^{15}NO_3^-$ observations is compiled from previous studies and compared to the model results on a regional basis where sufficient observations exist. The model is able to qualitatively and quantitatively reproduce many of the observed patterns such as high subsurface values in water column denitrification zones and the meridional and vertical gradients in the Southern Ocean. The observed pronounced subsurface minimum in the Atlantic is underestimated by the model presumably owing to too little simulated nitrogen fixation there. Sensitivity experiments reveal that algal NO_3^- uptake, nitrogen fixation, and water column denitrification have the strongest effects on the simulated distribution of nitrogen isotopes, whereas the effect from zooplankton excretion is weaker. Both water column and sedimentary denitrification also have important indirect effects on the nitrogen isotope distribution by reducing the fixed nitrogen inventory, which creates an ecological niche for nitrogen fixers and, thus, stimulates additional N_2 fixation in the model. Important model deficiencies are identified, and strategies for future improvement and possibilities for model application are outlined.

Citation: Somes, C. J., A. Schmittner, E. D. Galbraith, M. F. Lehmann, M. A. Altabet, J. P. Montoya, R. M. Letelier, A. C. Mix, A. Bourbonnais, and M. Eby (2010), Simulating the global distribution of nitrogen isotopes in the ocean, *Global Biogeochem. Cycles*, *24*, GB4019, doi:10.1029/2009GB003767.

1. Introduction

[2] Bioavailable nitrogen (fixed N) is one of the major limiting nutrients for algal photosynthesis, which drives the sequestration of CO_2 from the surface ocean and atmosphere into the deep ocean via the sinking of organic matter. Changes in this so-called "biological pump" have been hypothesized to account for a significant amount of the glacial-interglacial fluctuations in atmospheric CO_2 [*McElroy*, 1983; *Falkowski*, 1997]. However, the relative contributions of the biological and physical carbon pumps to CO_2 variations remain controversial. The size of the oceanic fixed N inventory, which regulates the strength of the biological pump, is controlled by different biogeochemical processes that are difficult to constrain quantitatively in a global budget [*Codispoti*, 2007]. Nitrogen isotopes (both in dissolved and organic N species) in the water column and seafloor sediments are sensitive indicators of those processes [*Brandes and Devol*, 2002; *Deutsch et al.*, 2004; *Altabet*, 2007].

[3] Many N transformational processes alter the ratio of the two stable forms of the nitrogen isotopes, ^{14}N and ^{15}N, differently, a process referred to as fractionation. Resulting variations in N isotopic composition can be described as deviations in $^{15}N/^{14}N$ ratio from an accepted standard

$$\delta^{15}N = \left[\left(^{15}N/^{14}N\right)/R_{std} - 1\right] \times 1000, \quad (1)$$

where R_{std} is the $^{15}N/^{14}N$ ratio of atmospheric N_2 gas. Isotope fractionation can occur due to kinetic processes (i.e.,

[1]College of Oceanic and Atmospheric Sciences, Oregon State University, Corvallis, Oregon, USA.
[2]Department of Earth and Planetary Science, McGill University, Montreal, Quebec, Canada.
[3]Institute for Environmental Geoscience, University of Basel, Basel, Switzerland.
[4]School for Marine Science and Technology, University of Massachusetts Dartmouth, North Dartmouth, Massachusetts, USA.
[5]School of Biology, Georgia Institute of Technology, Atlanta, Georgia, USA.
[6]School of Earth and Ocean Sciences, University of Victoria, Victoria, British Columbia, Canada.

0886-6236/10/2009GB003767

different reaction rates for isotopes in a reactant product stream). It generally results in the enrichment of the heavier ^{15}N isotope in the reaction substrate, and its depletion in the product. For example, preferential discrimination against ^{15}N relative to ^{14}N during algal NO_3^- assimilation results in net enrichment of ^{15}N in the residual NO_3^- and net depletion of ^{15}N in organic matter (OM). The degree of isotopic discrimination, or fractionation, for each process can be quantified with an enrichment factor, $\varepsilon = (^{14}k/^{15}k - 1) \times 1000$, where k is the specific reaction rate for each isotope [*Mariotti et al.*, 1981].

[4] The predominant source and sink terms of the oceanic fixed N inventory, N_2 fixation and denitrification, respectively, have their own distinct effects on the signature of the N isotopes in the ocean. N_2 fixing prokaryotes (diazotrophs) introduce bioavailable N into the ocean close to that of atmospheric N_2 ($\delta^{15}N \approx -2$–0‰) [*Delwiche and Steyn*, 1970; *Minagawa and Wada*, 1986; *Macko et al.*, 1987; *Carpenter et al.*, 1997]. *Trichodesmium*, one of the most important and best studied diazotrophs, bloom more frequently and extensively in warm (>25°C) surface water where rates of aeolian Fe deposition are high such as the North Atlantic, Indian, and North Pacific compared to areas of low Fe deposition such as the South Pacific where the abundance of *Trichodesmium* appears to be much lower [*Karl et al.*, 2002; *Carpenter and Capone*, 2008]. However, other unicellular diazotrophs have been observed to grow in cooler water near 20°C [*Needoba et al.*, 2007], and it has been suggested that they also may significantly contribute to the global N_2 fixation rate [*Zehr et al.*, 2001; *Montoya et al.*, 2004].

[5] Denitrification occurs under suboxic conditions ($O_2 < 5$ μmol/kg) in the water column and in the seafloor sediments. Here, microbes use NO_3^- instead of O_2 as the electron acceptor during respiration and convert it to gaseous forms of N (N_2O and N_2), which can then escape to the atmosphere [*Codispoti and Richards*, 1976]. The volume and distribution of suboxic water is affected by the temperature-dependent solubility of O_2 at the surface and the rate of subduction of oxygen-saturated water masses to greater depths, as well as the amount of organic matter that remineralizes in the ocean interior, both of which are sensitive to changes in climate. Anammox is another important process that occurs in anaerobic conditions and eliminates forms of fixed N (NO_2^-, NH_4^+) in the water column by converting them into N_2 gas [*Mulder et al.*, 1995; *Thamdrup and Dalsgaard*, 2002; *Kuypers et al.*, 2003]. It has been suggested that anammox may even eliminate more fixed N than water column denitrification in some oxygen minimum zones [*Kuypers et al.*, 2005; *Lam et al.*, 2009], but just how important of a role anammox plays in the global fixed N inventory has yet to be determined.

[6] Denitrifiers preferentially consume $^{14}NO_3^-$ leaving the residual oceanic NO_3^- pool strongly enriched in the heavier ^{15}N, with N isotope enrichment factors between 20–30‰ [*Cline and Kaplan*, 1975; *Liu and Kaplan*, 1989; *Brandes et al.*, 1998; *Altabet et al.*, 1999b; *Voss et al.*, 2001]. Sedimentary denitrification is generally limited by the amount of NO_3^- that diffuses into the reactive zones within the sediments. Therefore, it consumes nearly all of the influxing NO_3^- available, leaving nearly unaltered $\delta^{15}N$ values in the overlying waters [*Brandes and Devol*, 1997, 2002; *Sigman et al.*, 2003; *Lehmann et al.*, 2004, 2007]. The average oceanic $\delta^{15}NO_3^-$ value near 5‰ [*Sigman et al.*, 1997, 1999] can be interpreted as the balance between the isotope effects of water column denitrification, sedimentary denitrification, and N_2 fixation [*Brandes and Devol*, 2002; *Deutsch et al.*, 2004; *Galbraith et al.*, 2004; *Altabet*, 2007].

[7] The $\delta^{15}N$ signal in the water column and seafloor sediments is also affected by fractionation processes within the food chain. Marine algae preferentially assimilate the lighter ^{14}N into their biomass with a range of enrichment factors estimated in the field between 4–15‰ [*Wada*, 1980; *Altabet et al.*, 1991, 1999b; *Sigman et al.*, 1999; *Altabet and Francois*, 2001; *Karsh et al.*, 2003; *DiFiore et al.*, 2006]. Nitrogen is not lost or gained from the ocean during algal NO_3^- assimilation, but the spatial separation between net assimilation and remineralization can cause a trend of decreasing $\delta^{15}NO_3^-$ with depth. Distinguishing between the different isotope effects remains a challenge, especially in regions where multiple N transformational processes are occurring within close proximity.

[8] This study, for the first time to our knowledge, includes a dynamic nitrogen isotope module embedded within an existing global ocean-atmosphere-sea ice-biogeochemical model. This allows a direct comparison with nitrogen isotope observations, whereas previous box model studies could only be used more qualitatively [*Giraud et al.*, 2000; *Deutsch et al.*, 2004]. We provide a detailed description of the nitrogen isotope model and an assessment of its skill in reproducing present-day $\delta^{15}NO_3^-$ observations. Comparison of model results with $\delta^{15}N$ observations will also be used to help to quantify processes that affect the global oceanic distribution of $\delta^{15}N$. Sensitivity experiments illustrate the individual isotope effects of different processes on the spatial distribution of the N isotopes. In combination with measurements in ocean sediments and in the water column, the model can be a tool to better understand variations of $\delta^{15}N$ and the nitrogen cycle in the past and present.

2. Model Description

2.1. Physical Model

[9] The physical model is based on the University of Victoria Earth system climate model [*Weaver et al.*, 2001], version 2.8. It includes a global, three-dimensional general circulation model of the ocean (Modular Ocean Model 2) with physical parameterizations such as diffusive mixing along and across isopycnals, eddy induced tracer advection [*Gent and McWilliams*, 1990] and a scheme for the computation of tidally induced diapycnal mixing over rough topography [*Simmons et al.*, 2004]. Nineteen vertical levels are used with a horizontal resolution of 1.8° × 3.6°. To improve the simulation of equatorial currents, we have increased the meridional resolution in the tropics to 0.9° (between 10°S and 10°N and smoothly transitioning to 1.8° at 20°N/S) and added an anisotropic viscosity scheme [*Large et al.*, 2001]. A more detailed description of this

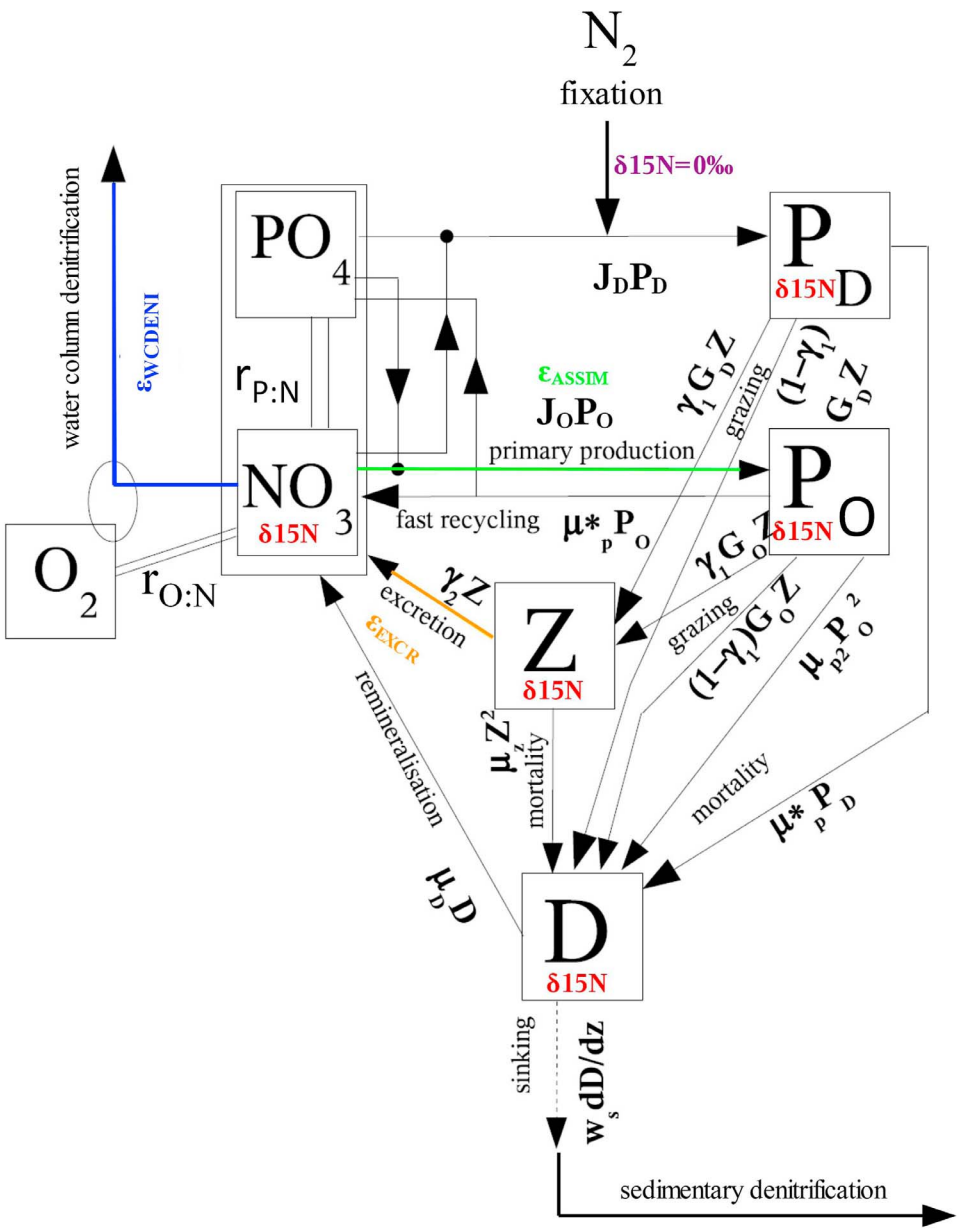

Figure 1. Schematic of the marine ecosystem model with the nitrogen isotope model parameters in color.

parameterization and its effect on the equatorial circulation is provided in Text S1 of the auxiliary material.[1] To account for the overestimated ventilation in the North Pacific, an artificial stratifying force equal to 0.04 Sv of freshwater is applied over the surface north of 55° in the Pacific and compensated elsewhere. A two dimensional, single level energy-moisture balance model of the atmosphere and a state-of-the-art dynamic-thermodynamic sea ice model are used, forced with prescribed NCEP/NCAR monthly climatological winds.

[1]Auxiliary materials are available in the HTML. doi:10.1029/2009GB003767.

2.2. Marine Ecosystem Biogeochemical Model

[10] The marine ecosystem model is an improved version of the 2N2PZD (2Nutrient, 2Phytoplankton, Zooplankton, Detritus) ecosystem model of [*Schmittner et al.*, 2008] (Figure 1). The organic variables include two classes of phytoplankton, N_2 fixing diazotrophs (P_D) and a "general" NO_3^- assimilating phytoplankton class (P_O), as well as zooplankton (Z) and organic detritus (D). The inorganic variables include dissolved oxygen (O_2) and two nutrients, nitrate (NO_3^-) and phosphate (PO_4^{3-}), both of which are consumed by phytoplankton and remineralized in fixed elemental ratios ($r_{N:P}$ = 16, $r_{O:P}$ = 170). We note, though,

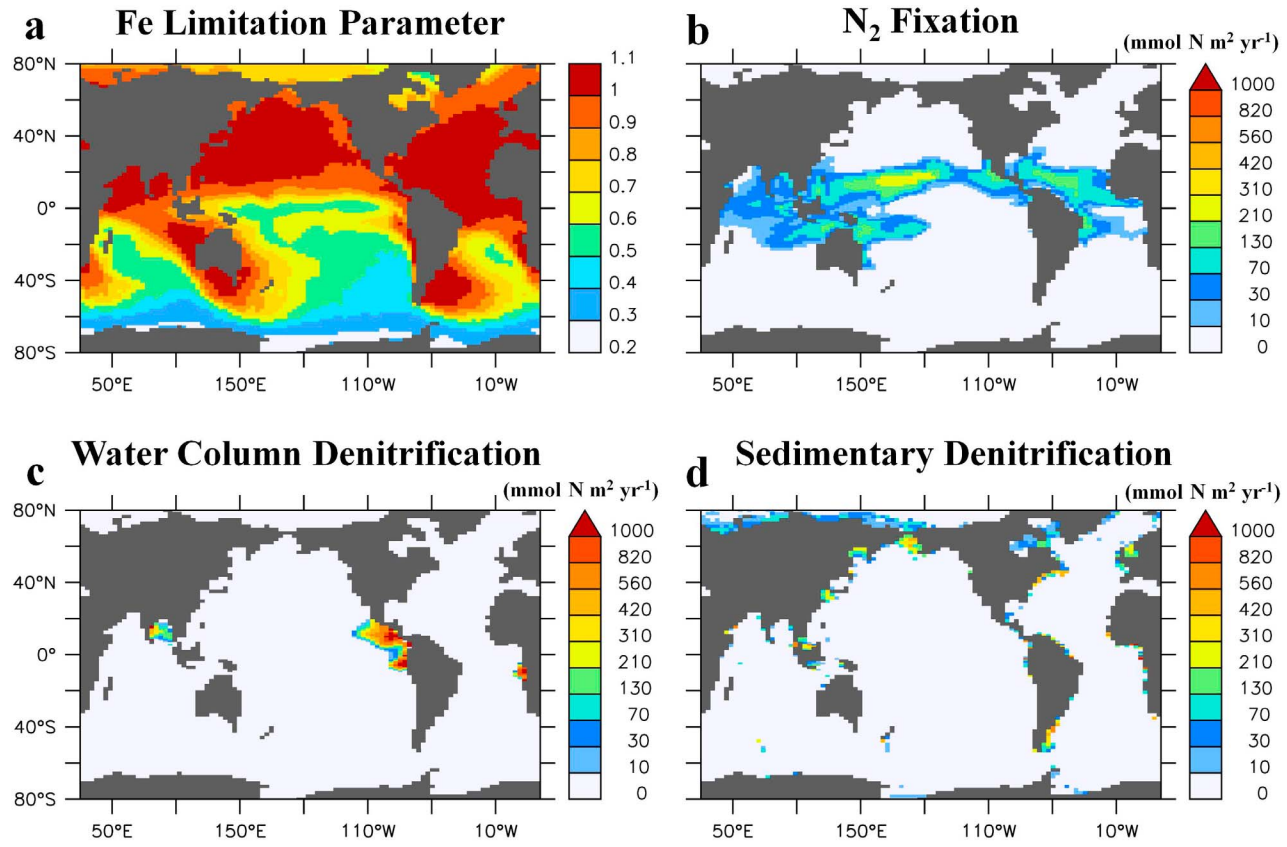

Figure 2. (a) Fe limitation parameter based on an estimate of aeolian dust deposition [*Mahowald et al.*, 2005] which is multiplied to the maximum growth rate of diazotrophs (see text). Annual vertically integrated rates of (b) N_2 fixation, (c) water column denitrification, and (d) sedimentary denitrification.

that most diazotrophs have been found to have a $r_{N:P}$ of 50:1 and sometimes higher [e.g., *Letelier and Karl*, 1996, 1998; *White et al.*, 2006]. This simplification is one of the reasons why the nitrogen surplus $N' = NO_3^- - 16PO_4^{3-}$ is generally underestimated in surface waters in the model (Figure S3). In addition to water column denitrification and N_2 fixation, we now include a parameterization for sedimentary denitrification (see auxiliary material equation (S11) and Figure 2), based on the flux of organic carbon into the seafloor sediments [*Middelburg et al.*, 1996]. Since the model underestimates coastal upwelling, which drives large fluxes of organic carbon to the seafloor sediments, this parameterization is tuned to fit the global mean $\delta^{15}NO_3^-$ of 5‰ by multiplying the sedimentary denitrification equation by a constant factor (α_{SD} = 4.5). Global rates of model N_2 fixation, water column denitrification, and sedimentary denitrification are 101, 67.5, and 38.3 Tg N yr^{-1}, respectively. The relatively low model sedimentary to water column denitrification ratio of ~1:2 compared to other estimates from one-box models ranging from ~1:1 [*Altabet*, 2007] to ~4:1 [*Brandes and Devol*, 2002] is mostly due to the "dilution effect" [*Deutsch et al.*, 2004], which reduces the "effective" fractionation effect of water column denitrification as NO_3^- is locally consumed, an effect not incorporated in one-box models. This results in a lower sedimentary to water column denitrification ratio needed to set the global mean $\delta^{15}NO_3^-$ to 5‰ (see section 4.2 for further discussion). The complete marine ecosystem model description is provided in Text S2 of the auxiliary material. A comparison of the global distribution of NO_3^-, O_2, and N' with World Ocean Atlas 2005 (WOA05) observations is shown in Figure S3.

[11] Suboxic water, where water column denitrification occurs, is present in three main locations of the present-day oceans: the Eastern Tropical North Pacific (ETNP), the Eastern Tropical South Pacific (ETSP) and the Arabian Sea (Figure S3). Deficiencies in the physical circulation model simulate suboxic water in only one of these locations, the ETNP. The physical circulation model integrates coastal upwelling over a horizontal extent that is too large (due to its coarse resolution), which results in the underestimation of upwelling, export production, and the remineralization of organic matter at depth. This bias leads to too high O_2 concentrations, larger than required for water column denitrification, in the ETSP and the Arabian Sea. Suboxia in the so-called "shadow zone" of the ETNP is simulated better and investigated more in section 4.2. In the model, some water column denitrification also occurs in the Bay of Bengal and off SW Africa (Figure 2c), which has not been observed in the real ocean. However, the anammox reaction,

Table 1. Nitrogen Isotope Model Enrichment Factors

Process	Symbol	Model Enrichment Factor (‰)	Field Estimates[a] (‰)
Algal NO_3 assimilation	ε_{ASSIM}	5	4–15
N_2 fixation	ε_{NFIX}	1.5	0–2
Excretion	ε_{EXCR}	6	3–6
Water column denitrification	ε_{WCD}	25	22–30
Sedimentary denitrification	ε_{SD}	0	0–4

[a]See Appendix A for references.

which also eliminates fixed N in the water column, has been found to occur off SW Africa [*Kuypers et al.*, 2005]. *Naqvi* [2008] measured low decomposition rates in the Bay of Bengal. Effective ballasting and scavenging of organic matter by the massive riverine input of terrestrial matter, an effect not included in the model, may prevent water column denitrification in the Bay of Bengal, which is close to suboxic.

[12] Diazotrophs grow according to the same principles as algal phytoplankton in the model (see Text S2), but we also account for some of their different characteristics. N_2 fixation breaks down of the triple N bond of N_2, which is energetically more costly than assimilating fixed N [*Holl and Montoya*, 2005]. Therefore, in the model, the growth rate of diazotrophs is lower than that of general phytoplankton. It is zero in waters cooler than 15°C and increases 40% slower with temperature than the growth rate of general phytoplankton. Diazotrophs are not limited by NO_3^- and will thrive in waters that are N deficient (i.e., low N′ as a result of denitrification) in which sufficient P and Fe are available. Denitrification and the propagation of N-deficient waters into the shallow thermocline by physical transport processes create an ecological niche for diazotrophs in the model, which stimulates N_2 fixation [*Tyrrell*, 1999].

[13] One of the most important and best studied diazotrophs, *Trichodesmium*, also has large iron (Fe) requirements for growth [*Sañudo-Wilhelmy et al.*, 2001]. Diazotrophs may depend on aeolian Fe in oligotrophic waters because deep pycnocline inhibits upward mixing of subsurface Fe-replete waters into the euphotic zone [*Falkowski*, 1997; *Karl et al.*, 2002]. Therefore, their growth rate is further reduced according to the *Fe Limitation* parameter (Figure 2a), where an estimate of aeolian dust deposition [*Mahowald et al.*, 2005] is scaled between 0–1 by multiplying it by a constant factor and setting the maximum value to 1. This is a simple parameterization of Fe limitation of diazotrophy and its full effects are described elsewhere [*Somes et al.*, 2010]. The majority of N_2 fixation in the model occurs in oligotrophic waters "downstream" of denitrification zones where sufficient Fe exists (i.e., via aeolian Fe deposition) (Figure 2b). The pattern of N_2 fixation (such as high values in the tropical/subtropical North Pacific, the western tropical/subtropical South Pacific, the western tropical/subtropical South Atlantic, the tropical/subtropical North Atlantic and the Indian Ocean) is mostly consistent with direct observations [e.g., *Karl et al.*, 2002; *Carpenter and Capone*, 2008], with estimates based on the observed NO_3^- deficit and simulated circulation [*Deutsch et al.*, 2007], as well as with results from a more complex ecosystem model [*Moore and Doney*, 2007]. However, N_2 fixation in our model does not extend northward of 25–30°N in the North Pacific and North Atlantic, whereas some observations show N_2 fixation as far north as 35–40°N [*Church et al.*, 2008; *Kitajima et al.*, 2009].

2.3. Nitrogen Isotope Model

[14] The nitrogen isotope model simulates the distribution of the two stable nitrogen isotopes, ^{14}N and ^{15}N, in all N species throughout the global ocean that are included in the marine ecosystem model. Five prognostic variables of $\delta^{15}N$ are embedded within the marine ecosystem model for all species containing nitrogen: NO_3^-, diazotrophs, algal phytoplankton, zooplankton and organic detritus (Figure 1). The 'isotope effect' is referred to in the following as the effect that each process has on the respective oceanic isotopic N pool, which depends on the $\delta^{15}N$ value of the substrate, the process-specific enrichment factor (ε), and the degree of utilization ($u_{substrate}$) of the substrate during the reaction:

$$\delta^{15}N_{product} = \delta^{15}N_{substrate} - \varepsilon(1 - u_{substrate}), \quad (2)$$

where $u_{substrate}$ is the fraction of the initial substrate used in the reaction. For example, if all of the available substrate is consumed in the reaction (i.e., $u_{substrate} = 1$), the product will incorporate the $\delta^{15}N$ value of the substrate, nullifying any potential fractionation. However, if the rate of utilization is low (i.e., $u_{substrate} \sim 0$), the product will incorporate a relatively light $\delta^{15}N$ value compared to the substrate by the designated enrichment factor (Table 1).

[15] The processes in the model that fractionate nitrogen isotopes are algal NO_3^- assimilation (ε_{ASSIM} = 5‰), zooplankton excretion (ε_{EXCR} = 6‰), and water column denitrification (ε_{WCD} = 25‰) (Table 1). Fractionation results in the isotopic enrichment of the more reactive, thermodynamically preferred, light ^{14}N into the product of each reaction by a process-specific fractionation factor. For a detailed discussion of nitrogen isotope fractionation dynamics see *Mariotti et al.* [1981]. Although little fractionation occurs during N_2 fixation in the model, it has an important effect on $\delta^{15}N$ by introducing relatively light atmospheric N_2 ($\delta^{15}N$ = 0‰) into the oceanic fixed N inventory. Sedimentary denitrification also has been observed to have little effect on the oceanic isotopic N pool because denitrifiers consume nearly all NO_3^- diffusing into the sediments [*Brandes and Devol*, 1997, 2002; *Lehmann et al.*, 2004, 2007]. In the model, there is no fractionation during sedimentary denitrification (ε_{SD} = 0‰), although this is a simplification of observations [*Lehmann et al.*, 2007]. Fractionation during the remineralization of organic matter is not included in the model. The complete nitrogen isotope model description is provided in Appendix A.

3. Nitrogen Isotope Model Results

[16] The model simulates complex spatial patterns of $\delta^{15}NO_3^-$ and $\delta^{15}N$ organic matter (OM) throughout the global ocean (Figure 3, top). Patterns of surface $\delta^{15}NO_3^-$ and subsurface $\delta^{15}N$ OM are similar but values are offset

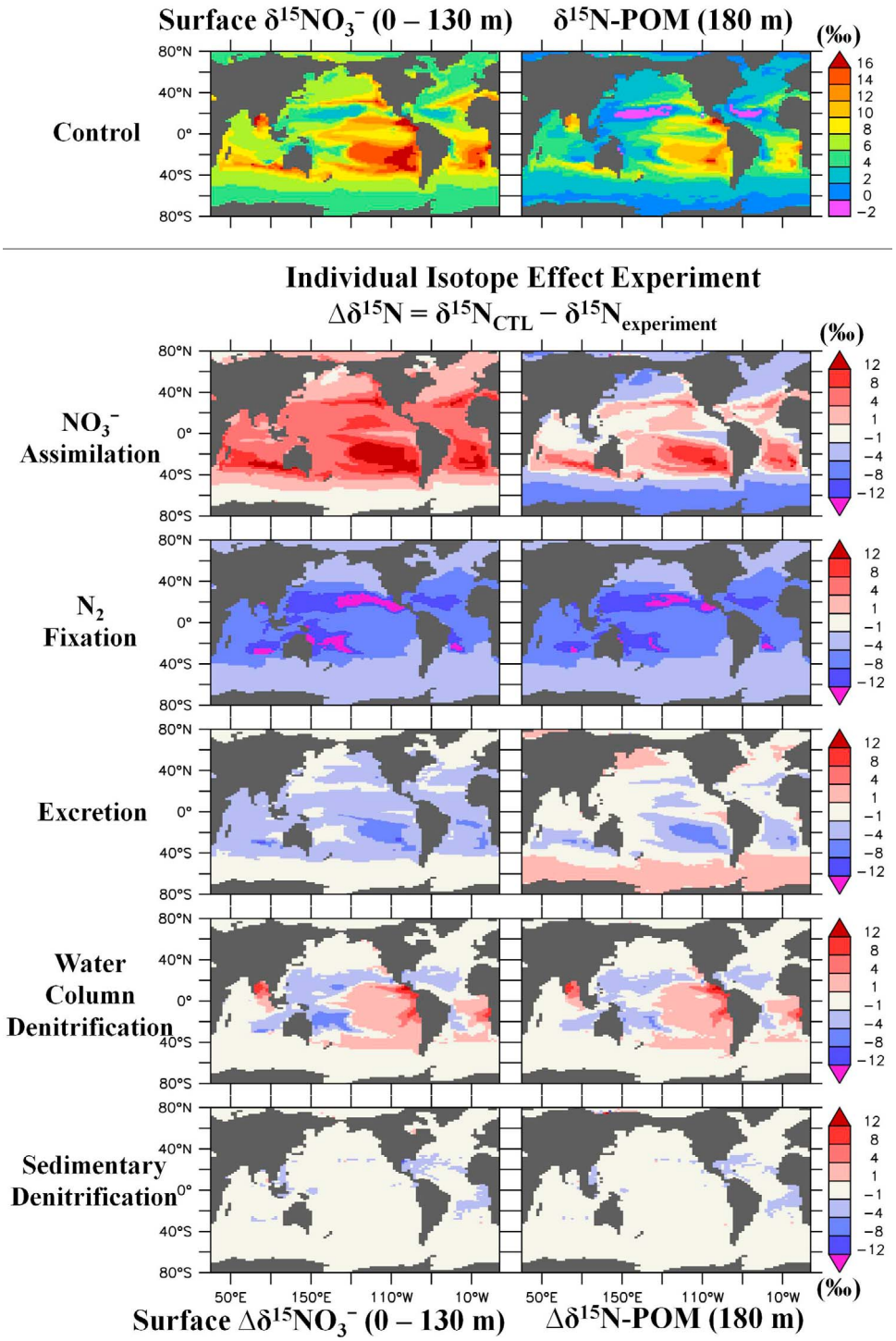

Figure 3. (top) Surface $\delta^{15}NO_3^-$ and $\delta^{15}N$ of sinking detritus in the model. (bottom) Isotope effect sensitivity experiments where one isotope effect is neglected per simulation and its difference with CTL is shown to illustrate its individual effect on the CTL simulation.

by two processes. First, as much as 5‰ offset due to fractionation during NO_3^- uptake by phytoplankton and second, by fractionation during zooplankton excretion, which increases the $\delta^{15}N$ OM through zooplankton mortality (Figure 1). High $\delta^{15}NO_3^-$ values (>15‰) are simulated in the eastern subtropical gyres, where surface NO_3^- is depleted, and in regions in close proximity to simulated suboxic zones in the Eastern Pacific, Bay of Bengal, and Eastern Atlantic

(again, note that water column denitrification has not been actually observed in the Bay of Bengal and Eastern Atlantic). A clear interhemispheric asymmetry appears between the subtropical gyres of the Pacific and Atlantic with higher values of 14–20‰ simulated in the southern hemisphere and smaller values of 10–14‰ in the northern hemisphere. More intermediate $\delta^{15}N$ values of 4–8‰ are found at high latitudes and near the equator where nutrient utilization is incomplete. $\delta^{15}N$ minima (<4‰) are located in the western tropical/subtropical ocean basins, where N_2 fixation occurs in the model (Figure 2b). The remainder of this section presents a more quantitative description of the contributions of individual processes to these relatively complex spatial patterns of $\delta^{15}NO_3^-$ and $\delta^{15}N$ OM.

[17] Figure 3 illustrates results from the full model (CTL) that includes all isotope effects (top panels) together with results from sensitivity experiments designed to isolate the effects of individual processes (bottom panels) on the global $\delta^{15}N$ distribution. This is accomplished by removing the isotope effect of one process per experiment and then calculating the difference ($\Delta\delta^{15}N$) with CTL. In the "NO_3^- Assimilation" and "Excretion" experiments, the enrichment factors ε_{ASSIM} and $\varepsilon_{EXCR,}$ respectively, are set to zero. In the "N_2 fixation" experiment the diazotroph's N isotope ratio is set equal to that of other phytoplankton at each location. In the "Water Column Denitrification" and "Sedimentary Denitrification" experiments, the entire process is switched off (thereby changing the global N inventory). These latter experiments also show the indirect effect that both denitrification processes have on $\delta^{15}N$ through the stimulation of N_2 fixation. In all other isotope effect experiments, the total N inventory does not change.

3.1. Algal NO_3^- Assimilation

[18] As phytoplankton preferentially assimilate $^{14}NO_3^-$ into organic matter, the residual inorganic N pool becomes enriched in $^{15}NO_3^-$. This creates an offset between surface $\delta^{15}NO_3^-$ and $\delta^{15}N$ OM that sinks toward the seafloor, which is set by the enrichment factor for NO_3^- assimilation (ε_{ASSIM} = 5‰) ("NO_3^- Assimilation" experiment, Figure 3). The surface NO_3^- utilization effect is also affected by the extent to which NO_3^- is depleted. When NO_3^- utilization is low (i.e., NO_3^--replete water exists), which occurs in High Nitrate Low Chlorophyll (HNLC) regions such as the Southern Ocean, the subarctic North Pacific, and the eastern equatorial Pacific, surface $\delta^{15}NO_3^-$ is determined by the source of $\delta^{15}NO_3^-$ being supplied to the surface. Algae will fractionate this NO_3^- during assimilation near the full extent set by the designated enrichment factor because of the abundance of available NO_3^-. In this oceanographic setting, the expected 5‰ difference between $\delta^{15}NO_3^-$ and $\delta^{15}N$ OM is almost fully expressed (i.e., $\delta^{15}N\text{-}P_O = \delta^{15}NO_3^- - \varepsilon_{ASSIM}$ with $u_{ASSIM} \approx 0$ in equation (2)). Thus, surface NO_3^- utilization in HNLC regions has a small influence on the surface $\delta^{15}NO_3^-$ signature, but play an important role for $\delta^{15}N$ OM that sinks out of the euphotic zone. This is perhaps most obvious in the Southern Ocean and in the subarctic North Pacific where $\Delta\delta^{15}NO_3^-$ is small, whereas $\Delta\delta^{15}N$ OM is strongly negative ("NO_3^- Assimilation" experiment, Figure 3).

[19] A different response is observed in oligotrophic regions where surface NO_3^- is depleted. Once the algae consume nearly all available NO_3^- (which itself becomes enriched in ^{15}N), they acquire the same N isotope signature from the source NO_3^- (i.e., $\delta^{15}N\text{-}P_O = \delta^{15}NO_3^-$ with u_{ASSIM} approaching 1). This drives the high $\delta^{15}N$ values in both NO_3^- and OM in the subtropics with maxima in the eastern poleward edges of the gyres (Figure 3). Although $\delta^{15}NO_3^-$ values are very high there, they have a small effect on $\delta^{15}N$ elsewhere because NO_3^- concentrations are very low. For instance, when low NO_3^- water mixes with nearby water with significantly higher NO_3^-, the resulting $\delta^{15}NO_3^-$ value will be weighted toward the water parcel containing more NO_3^- [see also *Deutsch et al.*, 2004]. This 'dilution effect' prevents high $\delta^{15}NO_3^-$ values in regions with high surface NO_3^- utilization from having a large impact on the $\delta^{15}NO_3^-$ signature across the nitracline.

3.2. Denitrification

[20] Denitrification only occurs at depth but its isotope effect can reach the surface due to upwelling and vertical mixing. Water column denitrification has a large enrichment factor and displays a very strong N isotope effect in close proximity to the simulated suboxic zones in the Eastern Pacific, Bay of Bengal, and Eastern Atlantic ("Water Column Denitrification" experiment in Figure 3). The unresolved poleward undercurrents along the western continental margin of the Americas (which could, in the real world, propagate high $\delta^{15}NO_3^-$ away from the subsurface suboxic zones [*Kienast et al.*, 2002]) may restrict the simulated water column denitrification isotope effect too much to regions proximal to the suboxic zones. Both water column and sedimentary denitrification also indirectly lead to lower $\delta^{15}NO_3^-$ values "downstream" of denitrification zones because they create N-deficient water that stimulates additional N_2 fixation, which introduces low $\delta^{15}N$ into the ocean. This negative feedback also decreases the horizontal extension of high $\delta^{15}NO_3^-$ signature originating from suboxic zones, because N_2 fixation introduces much lower $\delta^{15}N$ into the ocean.

3.3. N_2 Fixation

[21] The addition of newly fixed, isotopically light atmospheric N_2 ($\delta^{15}N_2 = 0$) by diazotrophs is the reason for the low $\delta^{15}N$ values in the western tropical/subtropical ocean basins. Since denitrification is the only process in the model that creates N-deficient water, and therefore an ecological niche for diazotrophs, the majority of N_2 fixation in the model occurs "downstream" of denitrification zones after phytoplankton have consumed all remaining surface NO_3^- and where sufficient aeolian Fe deposition exists. This low $\delta^{15}NO_3^-$ signature is evident in the subtropical North/South Pacific, the subtropical North/South Atlantic, and the Bay of Bengal ("N_2 Fixation" experiment, Figure 3).

3.4. Excretion

[22] According to our model results, the N isotope effect of excretion has a smaller influence on the simulated distribution of $\delta^{15}N$ in the global ocean ("Excretion" experiment, Figure 3) compared to the other processes discussed

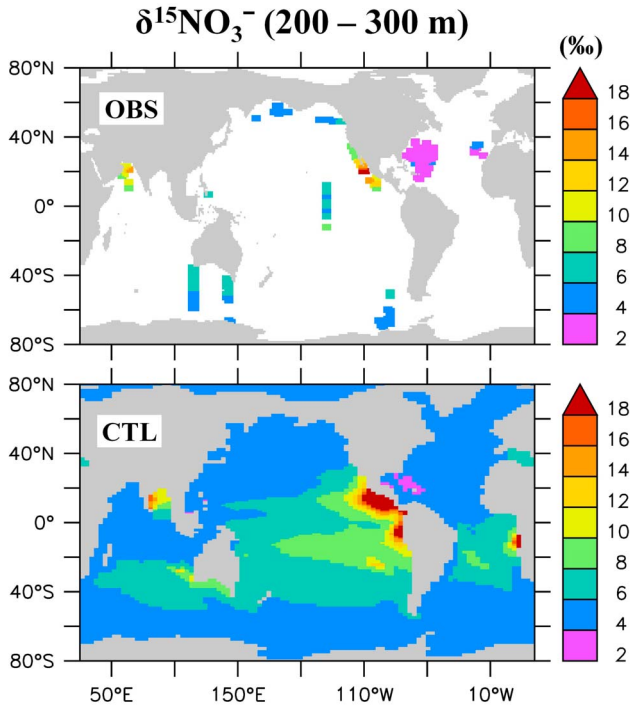

Figure 4. Comparison of annual $\delta^{15}NO_3^-$ (‰) averaged between 200 m and 300 m of available observations (OBS) and CTL. Because of the incomplete temporal coverage, seasonal biases in the annually averaged data exist depending on the region.

above. Its strongest effect is observed in the subtropical South Pacific, where NO_3^- is very low and excretion significantly contributes to the NO_3^- pool by introducing relatively low $\delta^{15}NO_3^-$. Low-latitude surface waters elsewhere are generally about 1–4‰ lighter due to fractionation during excretion, with little spatial gradients. At high latitudes the effect on $\delta^{15}NO_3^-$ is very small. We note that this N isotope effect is sensitive to the parameterization for excretion used in this marine ecosystem model version. The excretion rate was tuned so that $\delta^{15}N$ zooplankton is enriched by ~3.4‰ relative to phytoplankton [*Minagawa and Wada*, 1984].

4. Model Evaluation

[23] The relatively small number of $\delta^{15}N$ observations and the sparse spatial and temporal coverage make a full global model assessment difficult. However, certain regions have been sampled sufficiently to provide a meaningful comparison with the model results. All observations presented here are interpolated horizontally onto a 0.9° × 1.8° grid using a Gaussian weighted algorithm. The 33 depth levels are consistent with WOA05 and a linear interpolation is used for depths of missing data if nearby data exist. A global database of $\delta^{15}NO_3^-$ measurements has thus been constructed and is available for download (http://mgg.coas.oregonstate.edu/~andreas/Nitrogen/data.html). Figure 4 shows the annually averaged global distribution of measured $\delta^{15}NO_3^-$, averaged over 200–300 m depth to illustrate the spatial coverage. Seasonal sampling biases exist depending on the region. More details on the data sets can be found in the respective ocean region subsections that follow. Comparisons are presented for the Southern Ocean (Indian-Pacific sector), the Eastern Tropical North Pacific, and the Subtropical North Atlantic. Other regions with available $\delta^{15}NO_3^-$ observations included in the data set but not discussed in the text are the Bering Sea [*Lehmann et al.*, 2005], the Northeast Pacific [*Galbraith*, 2006], the Arabian Sea [*Altabet et al.*, 1999a], the Central Equatorial Pacific [*Somes et al.*, 2010], and the eastern Pacific sector of the Southern Ocean [*Sigman et al.*, 1999].

[24] Global measures of model performance for $\delta^{15}NO_3^-$ are presented in Table 2. These measures should be interpreted taken into account the highly localized nature of some of the processes as well as the limited regions covered by the database. A displacement in the location of denitrification, for example, will lead to a large decrease in the correlation coefficient and a large increase in the RMS errors. The CTL model has a correlation coefficient of 0.68, implying that the model explains 46% of the variance in the observations. The decrease of the correlation coefficient and the increase of the RMS error due to the neglection of a particular process can be regarded as the importance that this process plays in explaining the global $\delta^{15}NO_3^-$ observations of the database. The correlation coefficient measures the pattern of variability and neglects the absolute values, whereas the RMS error considers the deviation of the model from the observations in absolute values. Neglecting water column denitrification leads to the largest decrease in the correlation coefficient to 0.29 and to the second largest increase in the RMS error after N_2 fixation. Neglecting N_2 fixation and algal NO_3^- assimilation lead to the next largest decrease in the correlation coefficient. If sedimentary denitrification or excretion is not included, then the correlation coefficients decrease similarly, with both having relatively weaker effects on the distribution of $\delta^{15}NO_3^-$. Then, according to these measures, water column denitrification is the most important process determining the global $\delta^{15}NO_3^-$ distribution of available observations in the database, followed by N_2 fixation and algal NO_3^- assimilation, respectively. Finally, sedimentary denitrification and excretion are the least important.

4.1. Southern Indian-Pacific Ocean

[25] The Southern Ocean represents a critical region of biogeochemical cycling in the ocean because it is the largest open ocean region with incomplete drawdown of the major nutrients. This results in an excess amount of CO_2 at the

Table 2. Global Measures of $\delta^{15}NO_3^-$ Model Performance[a]

Model	*r*	*P*	RMS
Control	0.68	<0.0001	0.73
Algal NO_3 assimilation	0.60	0.00046	0.85
N_2 fixation	0.52	0.0026	2.1
Excretion	0.65	0.00010	0.80
Water column denitrification	0.29	0.12	1.1
Sedimentary denitrification	0.64	0.00010	0.82

[a]Correlation coefficient (*r*), correlation significance (*P*), and root mean squared (RMS) error normalized by the standard deviation of the observations.

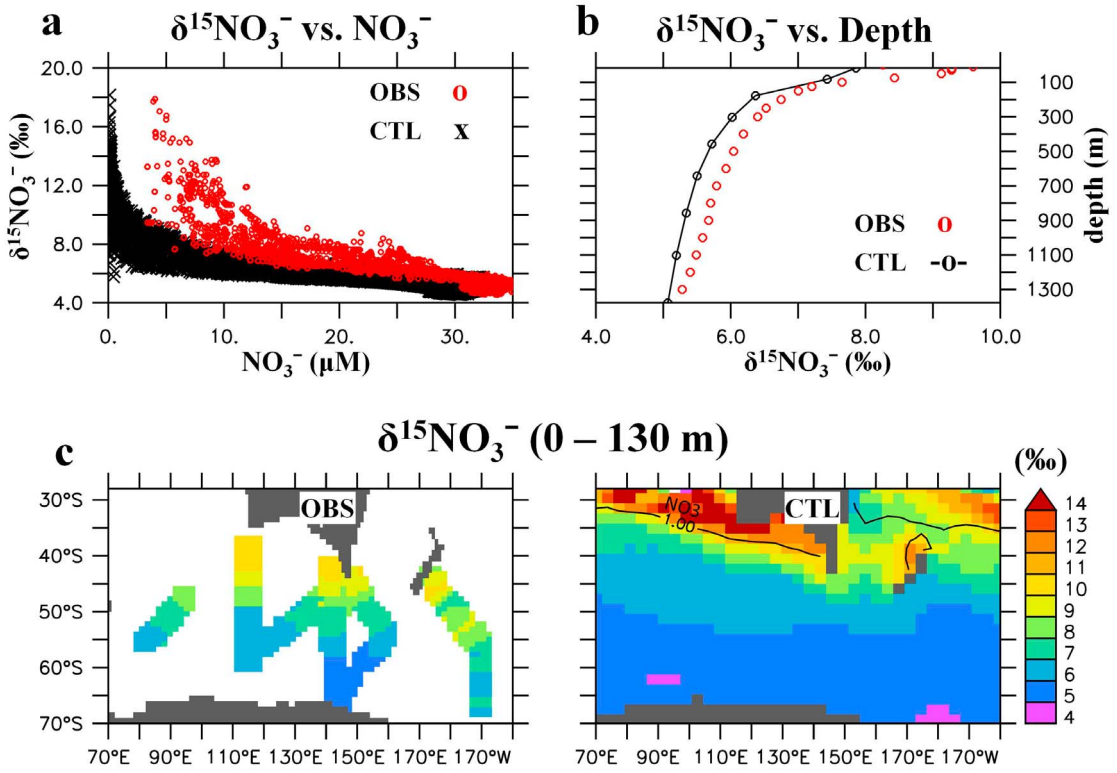

Figure 5. Comparison of the Indian-Pacific sector of the Southern Ocean with the $\delta^{15}NO_3^-$ database and CTL: (a) $\delta^{15}NO_3^-$ versus NO_3^-, (b) horizontally averaged (over available data) depth $\delta^{15}NO_3^-$ profiles, and (c) surface $\delta^{15}NO_3^-$ and with a 1μM NO_3^- contour line.

surface, which is released to the atmosphere (under preindustrial conditions). The degree to which surface nutrients are utilized here may have profound impacts on ocean-atmosphere exchanges of CO_2. Figure 5 shows a comparison with observations recorded in the region [*Sigman et al.*, 1999; *Altabet and Francois*, 2001; *DiFiore et al.*, 2006]. This data subset compiles observations from 8 cruises covering various seasons. Since all cruises do not cover the same location, some seasonal biases can be expected, yet, we still decided to use annual averages for maximum spatial coverage. Note the model does not simulate interannual variability due to the prescribed monthly climatological winds and temporally constant biogeochemical parameters.

[26] Qualitatively, the inverse trend of increasing $\delta^{15}NO_3^-$ with decreasing NO_3^- (Figure 5a) is reproduced by the model. However, the slope is underestimated suggesting that the enrichment factor for algal NO_3^- assimilation used in the model (ε_{ASSIM} = 5‰) is too low, in agreement with *DiFiore et al.* [2006] that suggests at least 7‰. The simulated vertical gradient is in good agreement with the observations. Deep water $\delta^{15}NO_3^-$ at 2000 m depth is around 5‰ and slowly increasing throughout the lower pycnocline to around 6‰ at 500 m depth. The model slightly underestimates $\delta^{15}NO_3^-$ between 100 m depth by ~0.2‰, whereas near surface values are underestimated by 1.5‰.

[27] The meridional gradient of observed surface $\delta^{15}NO_3^-$, with low values of ~5‰ at high latitudes and higher values of ~10‰ north of 45°S, are captured by the model, except that the gradient in the model is sharper and shifted northward by about 10°. Very high $\delta^{15}NO_3^-$ values are simulated north of ~40°S off the southern coast of Australia (Figure 5c). This is due to the fact that the model overestimates the utilization of surface NO_3^- relative to observations there (Figures 5c and S3). Where the simulated NO_3^- is almost completely consumed (i.e., NO_3^- < 1 μM) (see Figure 5c contour line), the remaining $\delta^{15}NO_3^-$ values become as high as 18‰. Since none of the existing $\delta^{15}NO_3^-$ observations was collected in such low NO_3^- concentrations (Figure 5a), it is impossible, at this time, to falsify this aspect of the N isotope model response. We note this heavy $\delta^{15}NO_3^-$ signature in these low NO_3^- waters has little effect on $\delta^{15}NO_3^-$ across the nitracline in the model because the $\delta^{15}N$ signature of very low NO_3^- water becomes diluted out as it mixes with much higher NO_3^- water (see section 3.1).

4.2. Eastern Tropical North Pacific

[28] The ETNP contains the largest suboxic zone in the ocean, where water column denitrification occurs. The relatively small spatial scale of suboxic zones makes them difficult for the model to simulate accurately and deficiencies in the coarse resolution physical model prevent it from fully resolving some important physical processes, especially in coastal regions. Underestimating coastal upwelling (due to coarse resolution) results in corresponding underestimation of primary production, organic matter remineralization, and O_2 consumption at depth. This is a major

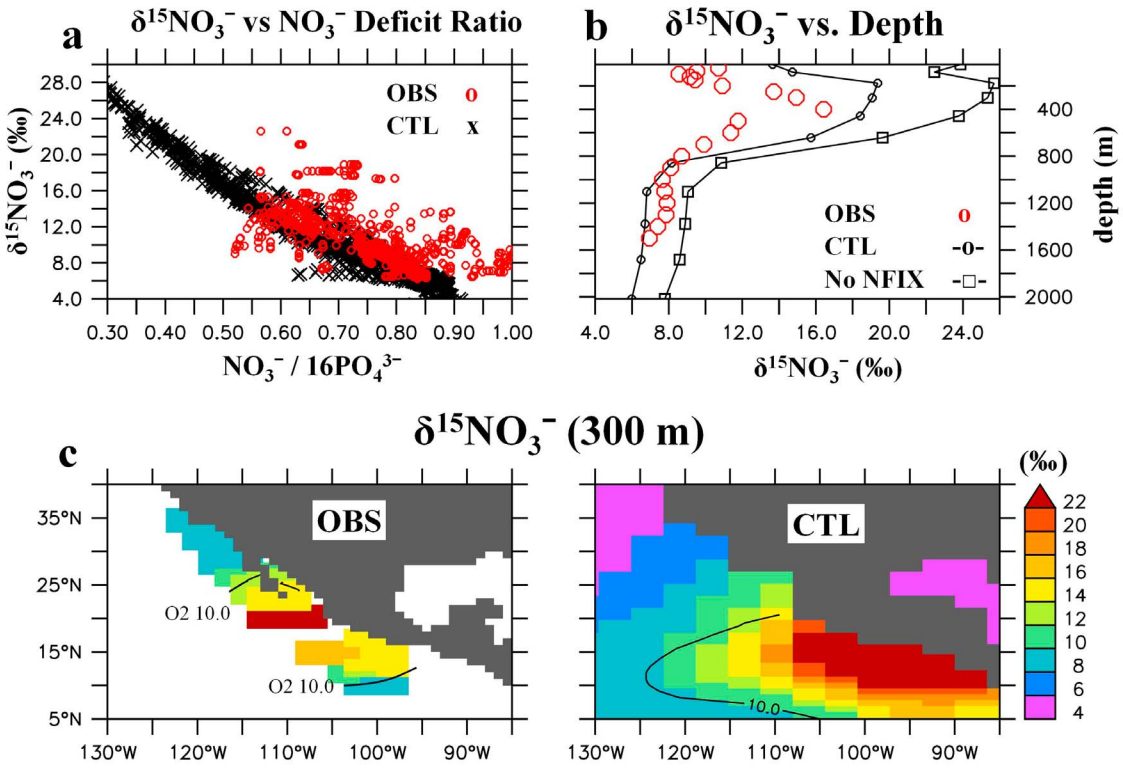

Figure 6. Comparison of the ETNP with the $\delta^{15}NO_3^-$ database and CTL: (a) $\delta^{15}NO_3^-$ versus N′ = $NO_3^- - 16PO_4^{3-}$, (b) horizontally averaged (within 10 μM O_2 contour) depth $\delta^{15}NO_3^-$ profiles including the experiment where the isotope effect of N_2 Fixation is neglected (no NFIX), and (c) subsurface $\delta^{15}NO_3^-$ with a 10 μM O_2 contour line.

reason for overestimated dissolved O_2 at depth in areas with significant coastal upwelling (e.g., off Peru and NW Mexico) (Figure S3), too large for water column denitrification to occur. Preliminary experiments suggest that increased vertical resolution can improve the simulation of productivity and suboxia in the Eastern Tropical South Pacific (not shown).

[29] The ability to reproduce the equatorial undercurrents that transport relatively oxygen-rich water from the western basin is also important for the simulation of the Eastern Pacific suboxic zones. The anisotropic viscosity scheme [*Large et al.*, 2001] improves equatorial dynamics considerably (Text S2 and Figure S1). The Pacific Equatorial Undercurrent increases from 0.15 m/s to nearly 0.8 m/s, just slightly weaker than observations, which show velocities near 1 m/s (Figure S2). The North Equatorial Countercurrent in the model also displays lower current velocities than observed, and does not deliver enough oxygen-rich water directly to the ETNP suboxic zone. This is likely the main reason why the simulated suboxic zone is too large and located too far south (by ~5°) relative to observations (Figure S3). This results in higher rates of water column denitrification and higher $\delta^{15}NO_3^-$ values, as well as more N-deficient water in the suboxic zone compared to observations (Figure 6).

[30] Since the locally high $\delta^{15}NO_3^-$ values exist in too small NO_3^- concentrations, when they transport out of the denitrification zone and mix with water with much higher NO_3^-, the high $\delta^{15}NO_3^-$ value is largely diluted away because the resulting $\delta^{15}NO_3^-$ value is weighted toward the water parcel with more NO_3^-. This "dilution effect" [*Deutsch et al.*, 2004] reduces the impact that water column denitrification has on $\delta^{15}NO_3^-$ outside of denitrification zones, and thus decreases its actual isotope effect on setting the global mean $\delta^{15}NO_3^-$. This is the main reason why the model requires a relatively low sedimentary to water column denitrification ratio of 1:2 to set the global mean $\delta^{15}NO_3^-$ to 5‰ compared to estimates from one-box models [*Brandes and Devol*, 2002; *Altabet*, 2007], which cannot account for any important effects that occur locally within the denitrification zone. However, note that our model significantly overestimates NO_3^- consumption via water column denitrification in the ETNP compared to observations (Figure 6a). Therefore, it is likely that our sedimentary to water column denitrification ratio of 1:2 is too low, but it does highlight the importance that the NO_3^- consumption/dilution effect can have on determining the global mean $\delta^{15}NO_3^-$.

[31] Figure 6 shows model $\delta^{15}NO_3^-$ compared to observational $\delta^{15}NO_3^-$ data collected during November 1999 [*Sigman et al.*, 2005] and October 2000 (M. Altabet, unpublished data, 2010). The model captures the general observed trend of increasing $\delta^{15}NO_3^-$ as NO_3^- is consumed during water column denitrification (Figure 6a). The model's too low N:P ratio for diazotrophs (r = 16:1 where

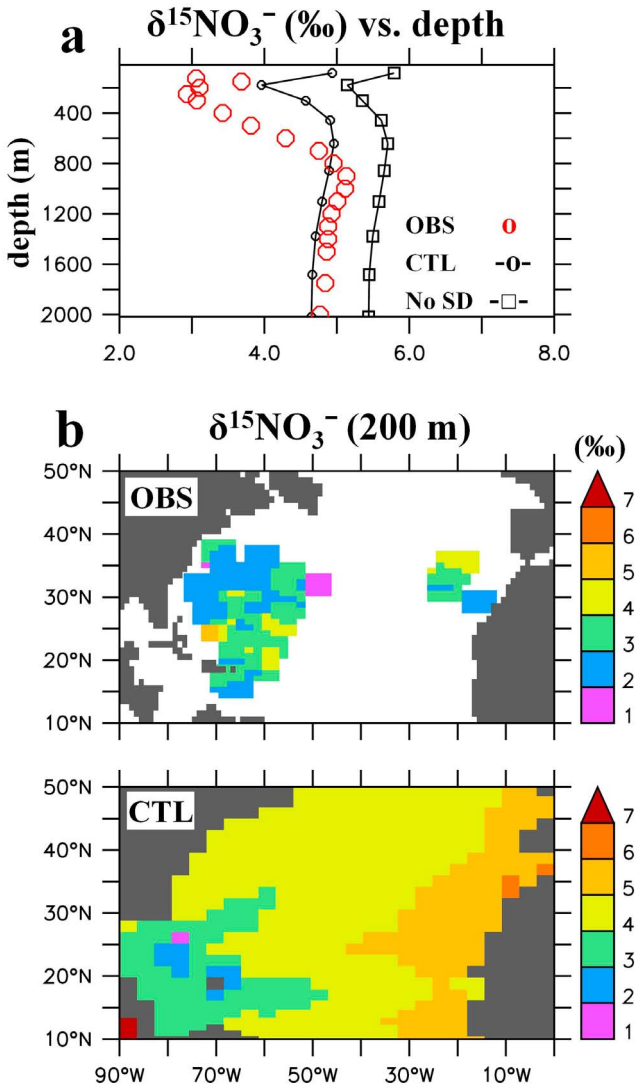

Figure 7. Comparison of the North Atlantic with the $\delta^{15}NO_3^-$ database and CTL. (a) Horizontally averaged (over available data) depth $\delta^{15}NO_3^-$ profiles including the experiment where sedimentary denitrification is neglected (no SD); (b) subsurface $\delta^{15}NO_3^-$.

observations show r = ~50:1 [*White et al.*, 2006; *Letelier and Karl*, 1996, 1998]) may partly explain its incapacity to simulate some of the relatively high N:P values of observations. The range of simulated values is also likely to be more limited compared to the observations due to the missing interannual and synoptic climate variability in the model. Figure 6b compares the horizontally averaged $\delta^{15}NO_3^-$ depth profiles only within the hypoxic zone (O_2 < 10 μM) at 300 m (contoured on Figure 6c) to account for the displaced OMZ. Within this region, the model is able to capture the general vertical distribution of $\delta^{15}NO_3^-$ seen in the measured data, such as the surface minimum and subsurface maximum.

[32] $\delta^{15}NO_3^-$ in the ETNP decreases toward the surface [*Cline and Kaplan*, 1975; *Brandes et al.*, 1998; *Voss et al.*, 2001; *Sigman et al.*, 2005] suggesting a source of isotopically light N at the surface. *Brandes et al.* [1998] proposed that in the Arabian Sea as much as 30% of primary production must be supported by N_2 fixation in order to account for the low surface $\delta^{15}NO_3^-$. Other observations also suggest that the decrease in $\delta^{15}NO_3^-$ toward the surface is likely due to the fixation of atmospheric N_2 and the subsequent, closely coupled remineralization-nitrification cycle [*Sigman et al.*, 2005]. We test this hypothesis by comparing the observations with the model experiment in which the isotope effect of N_2 fixation is neglected ("No NFIX"). In this case, the model overestimates surface $\delta^{15}NO_3^-$ by ~12‰ (Figure 6b) and the surface minimum is not simulated. This experiment demonstrates that the input of isotopically light fixed N from N_2 fixation in the model best explains the decreasing trend of $\delta^{15}NO_3^-$ observations toward the surface. In the model, 20% of the fixed N loss via denitrification is reintroduced into the surface by N_2 fixation occurring directly above the denitrification zone in the ETNP. The fact that the difference between the subsurface maximum and the near surface minimum is underestimated in the model (6‰ versus 8‰ in the observations) suggests that in the real world the locally reintroduced fraction could be larger than 20%.

4.3. North Atlantic

[33] Uncertainties regarding processes that can affect the nitrogen isotope signal make it challenging to interpret and simulate nitrogen isotopes in the North Atlantic. Estimates of atmospheric N deposition [*Duce et al.*, 2008] and the assimilation-remineralization-nitrification cycle are not well constrained. Although atmospheric N deposition may be significant in this region [*Michaels et al.*, 1996; *Lipschultz et al.*, 2002; *Knapp et al.*, 2005, 2008], its isotopic composition is not well known and therefore is not included in the model at this time. Figure 7 shows the comparison of annual model $\delta^{15}NO_3^-$ with available observations from cruises in May 2001 and 2004 (M. Altabet and J. P. Montoya, unpublished data, 2010), October 2002 [*Knapp et al.*, 2008], and May 2005 [*Bourbonnais et al.*, 2009]. The model overestimates the $\delta^{15}NO_3^-$ values everywhere, by 0.9‰ on average and by 2‰ at 200 m depth, presumably due mostly to the underestimation of N_2 fixation, but possibly also because atmospheric N deposition and/or fractionation during the remineralization of organic matter are not included. Both of these processes would act to decrease subsurface values of $\delta^{15}NO_3^-$. Underestimated N′ in the North Atlantic (Figure S3) also indicates too little N_2 fixation, but we again note the too low N:P ratio for diazotrophs also contributes to this N′ underestimation to some degree.

[34] N_2 fixation is most likely underestimated in the model because it does not consider dynamic elemental cycling of the microbial loop. It has been suggested that DOP is more labile relative to DON and recycles through the microbial loop more efficiently, which can help relieve diazotrophs of P limitation in this region and enhance N_2 fixation [*Wu et al.*, 2000]. The model is able to reproduce the pattern of low $\delta^{15}NO_3^-$ in the thermocline qualitatively, just not quantitatively to the extent present in the observations. Sedimentary denitrification in the North Atlantic sti-

mulates enough N_2 fixation in the model to generate a subsurface $\delta^{15}NO_3^-$ minimum. When sedimentary denitrification is switched off ("No SD"), the thermocline minimum is weaker and agrees less with the observations. This suggests that sedimentary denitrification is an important factor influencing N_2 fixation in the Subtropical North Atlantic, but not the only factor.

5. Discussion and Conclusions

[35] A new model of nitrogen isotopes has been implemented into the three-dimensional ocean component of a global Earth system climate model capable of millennial timescale simulations. Despite some model deficiencies, we have shown that this model can successfully reproduce the general spatial patterns of $\delta^{15}NO_3^-$ measured in the ocean. Sensitivity experiments allowed us to isolate the individual N isotope effects of various N transformational processes on the global distribution of $\delta^{15}N$. Algal NO_3^- assimilation, water column denitrification, and N_2 fixation all have strong influences in setting the global patterns of $\delta^{15}NO_3^-$ in the ocean, whereas the effect of zooplankton excretion is weaker.

[36] These simulations show that the isotope effect of algal NO_3^- assimilation can drive very large spatial gradients in both $\delta^{15}NO_3^-$ and $\delta^{15}N$ OM depending on the ocean environment (Figure 3). In HNLC areas where surface NO_3^- utilization is low and algae are able to fractionate NO_3^- at their designated enrichment factor, the $\delta^{15}N$ OM signature decreases. However, when NO_3^- utilization is high, the $\delta^{15}N$ OM signature is more similar to the $\delta^{15}NO_3^-$ value it consumes because the effective degree of fractionation becomes much lower (see section 3.1). Surface NO_3^- utilization gradients can transition rapidly, for example due to changes in ocean circulation or atmospheric Fe deposition, and can possibly drive large and rapid changes in $\delta^{15}NO_3^-$ and $\delta^{15}N$ OM. The important influence of surface NO_3^- utilization on the global distribution of N isotopes in the model suggests that changes in surface NO_3^- utilization patterns throughout Earth's history could contribute to large fluctuations in $\delta^{15}N$ observed in sediment records, especially near fronts where large surface NO_3^- gradients exist [see also *Altabet and Francois*, 1994; *Farrell et al.*, 1995; *Sigman et al.*, 1999; *Brunelle et al.*, 2007; *Galbraith et al.*, 2008; *Robinson and Sigman*, 2008].

[37] The model simulates a strong direct and indirect isotope effect of denitrification. High $\delta^{15}NO_3^-$ produced by water column denitrification has clear regional impacts and is also responsible for overall elevated $\delta^{15}NO_3^-$ of the ocean relative to the N_2 fixation source (see below). The indirect effect of both water column and sediment denitrification is mediated by the production of N-deficient water, which creates an ecological niche for diazotrophs. This stimulates additional N_2 fixation when other suitable conditions for N_2 fixation also exist (e.g., warm (>20°C), N-depleted water with sufficient P and Fe). This indirect effect also attenuates the horizontal circulation of high $\delta^{15}NO_3^-$ waters, originating from regions of water column denitrification, which causes its direct isotope effect to be regionalized near suboxic zones in the model.

[38] Key features of the model have been identified that are in need of further development. The coarse resolution physical circulation model does not fully resolve the dynamics of coastal upwelling regimes, which in part drive the flux of organic matter toward the seafloor sediments and its remineralization in the water column, as well as indirectly influences ventilation of suboxic zones. This is critical in the simulation of water column denitrification and sedimentary denitrification, which are important processes with respect to the global N isotope balance. Future model versions will include additional vertical levels to better resolve continental shelves as well as higher horizontal resolution. The model neglects dynamic elemental stoichiometry such as high N:P ratios of diazotrophs and the more efficient recycling of DOP relative to DON in microbial loops, which can help relieve diazotrophs of their P limitation and allow them to fix additional N_2 into the oceanic fixed N pool in oligotrophic waters. The ecosystem model also suffers from the exclusion of Fe as a prognostic tracer preventing it from being able to simulate differences in ecosystems limited by marconutrients (NO_3^-, PO_4^{3-}) versus micronutrients (Fe).

[39] Future applications of this model will include simulations of past climates, and direct comparison with $\delta^{15}N$ sediment records will be used to test the model results. This approach may be useful to quantify past interactions between the marine N cycle and its isotopes, as well as their impact on climate, and may provide new insights into important physical and biogeochemical changes throughout Earth's history.

Appendix A: Nitrogen Isotope Model

[40] The open system fractionation equation is used for fractionation during algal NO_3^- assimilation [*Altabet and Francois*, 2001]:

$$\delta^{15}N\text{-}P_O = \delta^{15}NO_3^- - \varepsilon_{ASSIM}(1 - u_{NO3}), \qquad (A1)$$

where $\delta^{15}N\text{-}P_O$ is the $\delta^{15}N$ of phytoplankton biomass assimilated during one time step, Δt, and u_{NO3} is the fraction of available NO_3^- that is converted into biomass ($u_{ASSIM} = J_O P_O \times \Delta t/NO_3^-$). When algae assimilate all available NO_3^- into their biomass (i.e., $u_{ASSIM} = 1$) they will incorporate the same $\delta^{15}N$ value as that of the source material. Many studies have estimated the fractionation factor in both laboratory and ocean environments. A wide variety of values have been reported in culture settings ranging from 0.7‰ to 23‰ [*Wada and Hattori*, 1978; *Montoya and McCarthy*, 1995; *Waser et al.*, 1998; *Needoba et al.*, 2003; *Granger et al.*, 2004]. A more confined range has been observed in field estimates from 4‰ to 15‰ [*Wada*, 1980; *Altabet et al.*, 1991, 1999b; *Sigman et al.*, 1999; *Altabet and Francois*, 2001; *Karsh et al.*, 2003; *DiFiore et al.*, 2006]. In our model we choose a constant value of 5‰ which is near the majority of estimates, although it is important to bear in mind the uncertainty in the parameter choice and the possibility that it varies in space and time.

[41] Nitrate in suboxic waters have been observed to have much higher $\delta^{15}N$ values due to fractionation during denitrification. Observations from present-day suboxic zones in

the Eastern Tropical North Pacific (ETNP) and the Arabian Sea (AS) have reported fractionation factors ranging from 22 to 30‰ [*Cline and Kaplan*, 1975; *Liu and Kaplan*, 1989; *Brandes et al.*, 1998; *Altabet et al.*, 1999b; *Voss et al.*, 2001]; we adopt a value of 25‰ in the model. Note that because these estimates were derived from field studies in which the isotope effect was estimated from the total nitrogen loss, they implicitly include the effect of anammox [*Galbraith et al.*, 2008]. Fractionation during denitrification is also simulated using the open system fractionation equation

$$\delta^{15}\mathrm{NO}_3^{\mathrm{OX}} = \delta^{15}\mathrm{NO}_3^- - \varepsilon_{\mathrm{WCD}}(1-u_{\mathrm{NO3}}), \tag{A2}$$

where $\mathrm{NO}_3^{\mathrm{OX}}$ is the oxygen-equivalent reduction of nitrate converted into N_2 gas during denitrification. The term u_{DENI} is the fraction of available NO_3 which is reduced into N_2 gas ($u_{\mathrm{NO3}} = \mu_{\mathrm{D}} D \times 0.8 \times r_{\mathrm{O:N}} \times \rho^{\mathrm{NO3}}{}_{\mathrm{sox}} \times L_{\mathrm{NO3}} \times \Delta t/\mathrm{NO}_3$).

[42] Excretion is the process responsible for the stepwise enrichment of δ^{15}N along the trophic chain in our model and is simulated using the instantaneous fractionation equation:

$$\delta^{15}\mathrm{NO}_3^- = \delta^{15}Z - \varepsilon_{\mathrm{EXCR}}. \tag{A3}$$

The instantaneous fractionation equation is used because excretion will always be a small fraction of the total zooplankton biomass and has been measured to be depleted by ~6‰ relative to its body [*Montoya*, 2008], which is the source of the excreted nitrogen. This leads to the average enrichment of ~3.4 per trophic level [*Minagawa and Wada*, 1984].

[43] Implementing these fractionation equations into the marine ecosystem model requires us to consider the exchanges of ^{14}N and ^{15}N between the various N pools separately. Total nitrogen abundance now has the form

$$\mathrm{N} = {}^{14}\mathrm{N} + {}^{15}\mathrm{N} \tag{A4}$$

for each variable in the isotope model. A fractionation coefficient is calculated for each process so the same equations for total N can be applied to ^{15}N [*Giraud et al.*, 2000]. For example, consider fractionation during algal NO_3^- assimilation. The isotopic ratio of new nitrogen biomass (P_O) is found using equations (1) and (2):

$$\delta^{15}N\text{-}P_O = \beta_{\mathrm{ASSIM}}\, \delta^{15}N\text{-}P_O \tag{A5}$$

where

$$\beta_{\mathrm{ASSIM}} = \frac{{}^{15}\mathrm{NO}_3}{{}^{14}\mathrm{NO}_3} - \frac{\varepsilon_{\mathrm{ASSIM}}(1-u_{\mathrm{NO3}})R_{std}}{1000}. \tag{A6}$$

[44] Applying equations (A4) and (A5) gives the amount of new $\delta^{15}N\text{-}P_O$ relative to the amount of total new nitrogen biomass, which is given by the primary production ($J_O P_O$), calculated by the marine ecosystem model:

$$\delta^{15}N\text{-}P_O = \frac{\beta_{\mathrm{ASSIM}}}{1+\beta_{\mathrm{ASSIM}}} J_O\, \delta^{15}N\text{-}P_O. \tag{A7}$$

Analogous derivations can be done for all fractionation coefficients. The time-dependent set of equations for ^{15}N which are embedded into the marine ecosystem model are as follows:

$$\frac{\partial^{15}\mathrm{NO}_3}{\partial t} = \left(R_D\mu_D D + \frac{\beta_{\mathrm{EXCR}}}{1+\beta_{\mathrm{EXCR}}}\gamma_2 Z + R_P\mu_P P_O - \frac{\beta_{\mathrm{ASSIM}}}{1+\beta_{\mathrm{ASSIM}}} J_O P_O - \frac{\beta_{\mathrm{ASSIM}}}{1+\beta_{\mathrm{ASSIM}}} u_N J_D P_D\right) \times \left[1 - \frac{\beta_{\mathrm{WCD}}}{1+\beta_{\mathrm{WCD}}} 0.8 R_{O:N}\rho^{\mathrm{NO3}}_{\mathrm{sox}} L_{\mathrm{NO3}}\right], \tag{A8}$$

$$\frac{\partial^{15}P_O}{\partial t} = \frac{\beta_{\mathrm{ASSIM}}}{1+\beta_{\mathrm{ASSIM}}} J_O P_O - R_P\mu_P P_O - R_{P_O} G(P_O) Z - R_{P_O}\mu_{P2} P_O^2, \tag{A9}$$

$$\frac{\partial^{15}N\text{-}P_D}{\partial t} = \left(\frac{\beta_{\mathrm{ASSIM}}}{1+\beta_{\mathrm{ASSIM}}} u_N + \frac{\beta_{\mathrm{NFIX}}}{1+\beta_{\mathrm{NFIX}}}(1-u_N)\right) J_D P_D + -R_{P_D} G(P_D) Z - R_{P_D}\mu_P P_D, \tag{A10}$$

$$\frac{\partial^{15}N\text{-}Z}{\partial t} = \gamma_1 [R_{P_O} G(P_O) + R_{P_D} G(P_D)] Z - \frac{\beta_{\mathrm{EXCR}}}{1+\beta_{\mathrm{EXCR}}}\gamma_2 Z - R_Z\mu_Z Z^2, \tag{A11}$$

$$\frac{\partial^{15}N\text{-}D}{\partial t} = (1-\gamma_1)[R_{P_O} G P_O + R_{P_D} G P_D] Z + R_{P_D}\mu_P P_D + R_{P_O}\mu_{P2} P_O^2 + R_Z\mu_Z Z^2 - R_D\mu_D D - R_D w_D \frac{\partial D}{\partial z}, \tag{A12}$$

where $R_{X\,=\,\mathrm{PO,\ PD,\ Z,\ D}} = {}^{15}\mathrm{N}/({}^{14}\mathrm{N} + {}^{15}\mathrm{N})$ is the ratio of heavy over total nitrogen. The complete parameter description is provided in Text S2. Here it suffices to note that the equations for total nitrogen (^{14}N + ^{15}N) are identical to the ones of ^{15}N except that $R_{\mathrm{X}} = \beta_{\mathrm{X}}/(1+\beta_{\mathrm{X}}) = 1$ in the total nitrogen equations.

[45] The model was carefully tested with zero fractionation in order to quantify and minimize numerical errors, which can occur for example due to slightly negative values of biological tracers caused by inaccuracies of the advection scheme. The biological code was adjusted to avoid negative concentrations as much as possible. Initially numerical errors in δ^{15}N ranged from ±1‰ in grid points at the seafloor to ±0.1‰ in the upper ocean. Setting $R_{\mathrm{std}} = 1$ instead of $R_{\mathrm{std}} = 0.0036765$, the actual atmospheric N_2 isotope ratio, reduces the numerical errors by over an order of magnitude. R_{std} is set to the value 1 so both isotope variables will be on the same order of magnitude. This prevents ^{15}N from becoming very close to zero as often, where inaccuracies of the advection scheme can cause it to be negative. This modification amounts to a scaling of ^{15}N and ^{14}N by a constant factor which does not affect the δ^{15}N dynamics. The remaining numerical errors of ±0.1‰ in the deep ocean and ±0.01‰ in the upper ocean are

2 orders of magnitude smaller than the observed variability. The model was integrated for over 5,000 years as it approaches equilibrium.

[46] **Acknowledgments.** We would like to thank Daniel Sigman, Angela Knapp, and Peter DiFiore for contributing data to this study. Reviews by two anonymous referees were appreciated. This work is funded by the Marine Geology and Geophysics program of the National Science Foundation (grant 0728315-OCE).

References

Altabet, M. A. (2007), Constraints on oceanic N balance/imbalance from sedimentary ^{15}N records, *Biogeosciences*, *4*, 75–86, doi:10.5194/bg-4-75-2007.

Altabet, M. A., and R. Francois (1994), Sedimentary nitrogen isotopic ratio as a recorder for surface ocean nitrate utilization, *Global Biogeochem. Cycles*, *8*(1), 103–116, doi:10.1029/93GB03396.

Altabet, M. A., and R. Francois (2001), Nitrogen isotope biogeochemistry of the Antarctic Polar Frontal Zone at 170W, *Deep Sea Res., Part II*, *48* (19–20), 4247–4273, doi:10.1016/S0967-0645(01)00088-1.

Altabet, M. A., W. G. Deuser, S. Honjo, and C. Stienen (1991), Seasonal and depth-related changes in the source of sinking particles in the North Atlantic, *Nature*, *354*, 136–139, doi:10.1038/354136a0.

Altabet, M. A., D. W. Murray, and W. L. Prell (1999a), Climatically linked oscillations in Arabian Sea denitrification over the past 1 m.y.: Implications for the marine N cycle, *Paleoceanography*, *14*(6), 732–743, doi:10.1029/1999PA900035.

Altabet, M. A., C. Pilskan, R. Thunell, C. Pride, D. Sigman, F. Chavez, and R. Francois (1999b), The nitrogen isotope biogeochemistry of sinking particles from the margin of the eastern North Pacific, *Deep Sea Res., Part I*, *46*, 655–679, doi:10.1016/S0967-0637(98)00084-3.

Bourbonnais, A., M. F. Lehmann, J. J. Waniek, and D. E. Schulz-Bull (2009), Nitrate isotope anomalies reflect N_2 fixation in the Azores Front region (subtropical NE Atlantic), *J. Geophys. Res.*, *114*, C03003, doi:10.1029/2007JC004617.

Brandes, J. A., and A. H. Devol (1997), Isotopic fractionation of oxygen and nitrogen in coastal marine sediments, *Geochim. Cosmochim. Acta*, *61*(9), 1793–1801, doi:10.1016/S0016-7037(97)00041-0.

Brandes, J. A., and A. H. Devol (2002), A global marine-fixed nitrogen isotopic budget: Implications for Holocene nitrogen cycling, *Global Biogeochem. Cycles*, *16*(4), 1120, doi:10.1029/2001GB001856.

Brandes, J. A., A. H. Devol, T. Yoshinari, D. A. Jayakumar, and S. W. A. Naqvi (1998), Isotopic composition of nitrate in the central Arabian Sea and eastern tropical North Pacific: A tracer for mixing and nitrogen cycles, *Limnol. Oceanogr.*, *43*(7), 1680–1689, doi:10.4319/lo.1998.43.7.1680.

Brunelle, B. G., D. M. Sigman, M. S. Cook, L. D. Keigwin, G. H. Haug, B. Plessen, G. Schettler, and S. L. Jaccard (2007), Evidence from diatom-bound nitrogen isotopes for subarctic Pacific stratification during the last ice age and a link to North Pacific denitrification changes, *Paleoceanography*, *22*, PA1215, doi:10.1029/2005PA001205.

Carpenter, E. J., and D. G. Capone (2008), Nitrogen fixation in the marine environment, in *Nitrogen in the Marine Environment*, edited by D. G. Capone et al., pp. 141–198, Elsevier, New York, doi:10.1016/B978-0-12-372522-6.00004-9.

Carpenter, E. J., H. R. Harvey, B. Fry, and D. G. Capone (1997), Biogeochemical tracers of the marine cyanobacterium *Trichodesmium*, *Deep Sea Res., Part I*, *44*(1), 27–38, doi:10.1016/S0967-0637(96)00091-X.

Church, M. J., K. M. Bjorkman, D. M. Karl, M. A. Saito, and J. P. Zehr (2008), Regional distributions of nitrogen-fixing bacteria in the Pacific Ocean, *Limnol. Oceanogr.*, *53*(1), 63–77.

Cline, J. D., and I. R. Kaplan (1975), Isotopic fractionation of dissolved nitrate during denitrification in the eastern tropical North Pacific Ocean, *Mar. Chem.*, *3*(4), 271–299, doi:10.1016/0304-4203(75)90009-2.

Codispoti, L. A. (2007), An oceanic fixed nitrogen sink exceeding 400 Tg N a^{-1} vs the concept of homeostasis in the fixed-nitrogen inventory, *Biogeosciences*, *4*, 233–253, doi:10.5194/bg-4-233-2007.

Codispoti, L. A., and F. A. Richards (1976), An analysis of the horizontal regime of denitrification in the eastern tropical North Pacific, *Limnol. Oceanogr.*, *21*(3), 379–388, doi:10.4319/lo.1976.21.3.0379.

Delwiche, C. C., and P. L. Steyn (1970), Nitrogen isotope fractionation in soils and microbial reactions, *Environ. Sci. Technol.*, *4*, 929–935, doi:10.1021/es60046a004.

Deutsch, C., D. M. Sigman, R. C. Thunell, A. N. Meckler, and G. H. Haug (2004), Isotopic constraints on glacial/interglacial changes in the oceanic nitrogen budget, *Global Biogeochem. Cycles*, *18*, GB4012, doi:10.1029/2003GB002189.

Deutsch, C., J. L. Sarmiento, D. M. Sigman, N. Gruber, and J. P. Dunne (2007), Spatial coupling of nitrogen inputs and losses in the ocean, *Nature*, *445*, 163–167, doi:10.1038/nature05392.

DiFiore, P. J., D. M. Sigman, T. W. Trull, M. J. Lourey, K. Karsh, G. Cane, and R. Ho (2006), Nitrogen isotope constraints on subantarctic biogeochemistry, *J. Geophys. Res.*, *111*, C08016, doi:10.1029/2005JC003216.

Duce, R. A., et al. (2008), Impacts of atmospheric anthropogenic nitrogen on the open ocean, *Science*, *320*(5878), 893–897, doi:10.1126/science.1150369.

Falkowski, P. G. (1997), Evolution of the nitrogen cycle and its influence on the biological sequestration of CO_2 in the ocean, *Nature*, *387*, 272–275, doi:10.1038/387272a0.

Farrell, J. W., T. F. Pedersen, S. E. Calvert, and B. Nielsen (1995), Glacial-interglacial changes in nutrient utilization in the equatorial Pacific Ocean, *Nature*, *377*, 514–517, doi:10.1038/377514a0.

Galbraith, E. G. (2006), Interactions between climate and the marine nitrogen cycle on glacial-interglacial timescales, Ph.D. thesis, Univ. of British Columbia, Vancouver.

Galbraith, E. G., M. Kienast, T. F. Pedersen, and S. E. Calvert (2004), Glacial-interglacial modulation of the marine nitrogen cycle by high-latitude O_2 supply to the global thermocline, *Paleoceanography*, *19*, PA4007, doi:10.1029/2003PA001000.

Galbraith, E. G., M. Kienast, S. L. Jaccard, T. F. Pedersen, B. G. Brunelle, D. M. Sigman, and T. Kiefer (2008), Consistent relationship between global climate and surface ntirate utilization in the western subarctic Pacific throughout the last 500 ka, *Paleoceanography*, *23*, PA2212, doi:10.1029/2007PA001518.

Gent, P. R., and J. C. McWilliams (1990), Isopycnal mixing in ocean circulation models, *J. Phys. Oceanogr.*, *20*, 150–155, doi:10.1175/1520-0485(1990)020<0150:IMIOCM>2.0.CO;2.

Giraud, X., P. Bertrand, V. Garcon, and I. Dadou (2000), Modeling d^{15}N evolution: First palaeoceanographic applications in a coastal upwelling system, *J. Mar. Res.*, *58*(4), 609–630, doi:10.1357/002224000321511043.

Granger, J., D. M. Sigman, J. A. Needoba, and P. J. Harrison (2004), Coupled nitrogen and oxygen isotope fractionation of nitrate during assimilation by cultures of marine phytoplankton, *Limnol. Oceanogr.*, *49*(5), 1763–1773, doi:10.4319/lo.2004.49.5.1763.

Holl, C. M., and J. P. Montoya (2005), Interactions between nitrate uptake and nitrogen fixation in continuous cultures of the marine diazotroph *Trichodesmium* (cyanobacteria), *J. Phycol.*, *41*, 1178–1183, doi:10.1111/j.1529-8817.2005.00146.x.

Karl, D., A. Michaels, B. Bergman, D. Capone, E. Carpenter, R. Letelier, F. Lipschultz, H. Paerl, D. Sigman, and L. Stal (2002), Dinitrogen fixation in the world's oceans, *Biogeochemistry*, *57–58*(1), 47–98, doi:10.1023/A:1015798105851.

Karsh, K. L., T. W. Trull, M. J. Lourey, and D. M. Sigman (2003), Relationship of nitrogen isotope fractionation to phytoplankton size and iron availability during the Southern Ocean Iron RElease Experiment (SOIREE), *Limnol. Oceanogr.*, *48*(3), 1058–1068, doi:10.4319/lo.2003.48.3.1058.

Kienast, S. S., S. E. Calvert, and T. F. Pedersen (2002), Nitrogen isotope productivity variations along the northeast Pacific margin over the last 120 kyr: Surface and subsurface paleoceanography, *Paleoceanography*, *17*(4), 1055, doi:10.1029/2001PA000650.

Kitajima, S., K. Furuya, F. Hashihama, S. Takeda, and J. Kanda (2009), Latitudinal distribution of diazotrophs and their nitrogen fixation in the tropical and subtropical western North Pacific, *Limnol. Oceanogr.*, *54*(2), 537–547.

Knapp, A. N., D. M. Sigman, and F. Lipschultz (2005), N isotopic composition of dissolved organic nitrogen and nitrate at the Bermuda Atlantic Time-series Study site, *Global Biogeochem. Cycles*, *19*, GB1018, doi:10.1029/2004GB002320.

Knapp, A. N., P. J. DiFiore, C. Deutsch, D. M. Sigman, and F. Lipschultz (2008), Nitrate isotopic composition between Bermuda and Puerto Rico: Implications for N_2 fixation in the Atlantic Ocean, *Global Biogeochem. Cycles*, *22*, GB3014, doi:10.1029/2007GB003107.

Kuypers, M. M. M., A. O. Sliekers, G. Lavik, M. Schmid, B. B. Jorgensen, J. G. Kuenen, J. S. S. Damste, M. Strous, and M. S. M. Jetten (2003), Anaerobic ammonium oxidation by anammox bacteria in the Black Sea, *Nature*, *422*, 608–611, doi:10.1038/nature01472.

Kuypers, M. M. M., G. Lavik, D. Woebken, M. Schmid, B. M. Bernhard, R. Amann, B. B. Jorgensen, and M. S. M. Jetten (2005), Massive nitrogen loss from the Benguela upwelling system through anaerobic ammo-

nium oxidation, *Proc. Natl. Acad. Sci. U. S. A.*, *102*(18), 6478–6483, doi:10.1073/pnas.0502088102.

Lam, P., G. Lavik, M. M. Jensen, J. van de Vossenberg, M. Schmid, D. Woebken, D. Gutierrez, M. S. M. Jetten, and M. M. M. Kuypers (2009), Revising the nitrogen cycle in the Peruvian oxygen minimum zone, *Proc. Natl. Acad. Sci. U. S. A.*, *106*(12), 4752–4757, doi:10.1073/pnas.0812444106.

Large, W. G., G. Danabasoglu, J. C. McWilliams, P. R. Gent, and F. O. Bryan (2001), Equatorial circulation of a global ocean climate model with anisotropic horizontal viscosity, *J. Phys. Oceanogr.*, *31*, 518–536, doi:10.1175/1520-0485(2001)031<0518:ECOAGO>2.0.CO;2.

Lehmann, M. F., D. M. Sigman, and W. M. Berelson (2004), Coupling the $^{15}N/^{14}N$ and $^{18}O/^{16}O$ of nitrate as a constraint on benthic nitrogen cycling, *Mar. Chem.*, *88*, 1–20, doi:10.1016/j.marchem.2004.02.001.

Lehmann, M. F., D. M. Sigman, D. C. McCorkle, B. G. Brunelle, S. Hoffmann, M. Kienast, G. Cane, and J. Clement (2005), Origin of the deep Bering Sea nitrate deficit: Constraints from the nitrogen and oxygen isotopic composition of water column nitrate and benthic nitrate fluxes, *Global Biogeochem. Cycles*, *19*, GB4005, doi:10.1029/2005GB002508.

Lehmann, M. F., D. M. Sigman, D. C. McCorkle, J. Granger, S. Hoffmann, G. Cane, and B. G. Brunelle (2007), The distribution of nitrate $^{15}N/^{14}N$ in marine sediments and the impact of benthic nitrogen loss on the isotopic composition of oceanic nitrate, *Geochim. Cosmochim. Acta*, *71*, 5384–5404, doi:10.1016/j.gca.2007.07.025.

Letelier, R. M., and D. M. Karl (1996), Role of Trichodesmium spp. in the productivity of the subtropical North Pacific Ocean, *Mar. Ecol. Prog. Ser.*, *133*, 263–273, doi:10.3354/meps133263.

Letelier, R. M., and D. M. Karl (1998), *Trichodesmium* spp. physiology and nutrient fluxes in the North Pacific subtropical gyre, *Aquat. Microb. Ecol.*, *15*, 265–276, doi:10.3354/ame015265.

Lipschultz, F., N. R. Bates, C. A. Carlson, and D. A. Hansell (2002), New production in the Sargasso Sea: History and current status, *Global Biogeochem. Cycles*, *16*(1), 1001, doi:10.1029/2000GB001319.

Liu, K.-K., and I. R. Kaplan (1989), The eastern tropical Pacific as a source of ^{15}N-enriched nitrate in seawater off southern California, *Limnol. Oceanogr.*, *34*(5), 820–830, doi:10.4319/lo.1989.34.5.0820.

Macko, S. A., M. L. Fogel, P. E. Hare, and T. C. Hoering (1987), Isotope fractionation of nitrogen and carbon in the synthesis of amino acids by microorganisms, *Chem. Geol. Isot. Geosci. Sect.*, *65*(1), 79–92, doi:10.1016/0168-9622(87)90064-9.

Mahowald, N. M., A. R. Baker, G. Bergametti, N. Brooks, R. A. Duce, T. D. Jickells, N. Kubilay, J. M. Prospero, and I. Tegen (2005), Atmospheric global dust cycle and iron inputs to the ocean, *Global Biogeochem. Cycles*, *19*, GB4025, doi:10.1029/2004GB002402.

Mariotti, A., J. C. Germon, P. Hubert, P. Kaiser, R. Letolle, A. Tardieux, and P. Tardieux (1981), Experimental determination of nitrogen kinetic isotope fractionation: Some principles; illustration for the denitrification and nitrification processes, *Plant Soil*, *62*(3), 413–430, doi:10.1007/BF02374138.

McElroy, M. B. (1983), Marine biological controls on atmospheric CO_2 and climate, *Nature*, *302*, 328–329, doi:10.1038/302328a0.

Michaels, A. F., D. Olson, J. L. Sarmiento, J. W. Ammerman, K. Fanning, R. Jahnke, A. H. Knap, F. Lipschultz, and J. M. Prospero (1996), Inputs, losses and transformations of nitrogen and phosphorus in the pelagic North Atlantic Ocean, in *Nitrogen Cycling in the North Atlantic Ocean and its Watersheds*, edited by R. W. Howarth, pp. 181–226, Kluwer Acad., Boston.

Middelburg, J. J., K. Soetaert, P. M. J. Herman, and C. H. R. Heip (1996), Denitrification in marine sediments: A model study, *Global Biogeochem. Cycles*, *10*(4), 661–673, doi:10.1029/96GB02562.

Minagawa, M., and E. Wada (1984), Stepwise enrichment of ^{15}N along food chains: Further evidence and the relation between $d^{15}N$ and animal age, *Geochim. Cosmochim. Acta*, *48*(5), 1135–1140, doi:10.1016/0016-7037(84)90204-7.

Minagawa, M., and E. Wada (1986), Nitrogen isotope ratios of red tide organisms in the East China Sea: A characterization of biological nitrogen fixation, *Mar. Chem.*, *19*(3), 245–259, doi:10.1016/0304-4203(86)90026-5.

Montoya, J. P. (2008), Nitrogen stable isotopes in marine environments, in *Nitrogen in the Marine Environment*, edited by D. G. Capone et al., pp. 1277–1302, Elsevier, New York, doi:10.1016/B978-0-12-372522-6.00029-3.

Montoya, J. P., and J. J. McCarthy (1995), Isotopic fractionation during nitrate uptake by phytoplankton grown in continuous culture, *J. Plankton Res.*, *17*(3), 439–464, doi:10.1093/plankt/17.3.439.

Montoya, J. P., C. M. Holl, J. P. Zehr, A. Hansen, T. A. Villareal, and D. G. Capone (2004), High rates of N_2 fixation by unicellular diazotrophs in the oligotrophic Pacific Ocean, *Nature*, *430*, 1027–1032, doi:10.1038/nature02824.

Moore, J. K., and S. C. Doney (2007), Iron availability limits the ocean nitrogen inventory stabilizing feedbacks between marine denitrification and nitrogen fixation, *Global Biogeochem. Cycles*, *21*, GB2001, doi:10.1029/2006GB002762.

Mulder, A., A. A. van de Graaf, L. A. Robertson, and J. G. Kuenen (1995), Anaerobic ammonium oxidation discovered in a denitrifying fluidized bed reactor, *FEMS Microbiol. Ecol.*, *16*(3), 177–184, doi:10.1111/j.1574-6941.1995.tb00281.x.

Naqvi, S. W. A. (2008), The Indian Ocean, in *Nitrogen in the Marine Environment*, edited by D. G. Capone et al., pp. 631–681, Elsevier, New York, doi:10.1016/B978-0-12-372522-6.00014-1.

Needoba, J. A., N. A. Waser, P. J. Harrison, and S. E. Calvert (2003), Nitrogen isotope fractionation in 12 species of marine phytoplankton during growth on nitrate, *Mar. Ecol. Prog. Ser.*, *255*, 81–91, doi:10.3354/meps255081.

Needoba, J. A., R. A. Foster, C. Sakamoto, J. P. Zehr, and K. S. Johnson (2007), Nitrogen fixation by unicellular diazotrophic cyanobacteria in the temperate oligotrophic North Pacific Ocean, *Limnol. Oceanogr.*, *52*(4), 1317–1327.

Robinson, R. S., and D. M. Sigman (2008), Nitrogen isotopic evidence for a poleward decrease in surface nitrate within the ice age Antarctic, *Quat. Sci. Rev.*, *27*(9–10), 1076–1090, doi:10.1016/j.quascirev.2008.02.005.

Sañudo-Wilhelmy, S. A., A. B. Kustka, C. J. Gobler, D. A. Hutchins, M. Yang, K. Lwiza, J. Burns, D. G. Capone, J. A. Raven, and E. J. Carpenter (2001), Phosphorus limitation of nitrogen fixation by *Trichodesmium* in the central Atlantic Ocean, *Nature*, *411*, 66–69, doi:10.1038/35075041.

Schmittner, A., A. Oschlies, H. D. Matthews, and E. G. Galbraith (2008), Future changes in climate, ocean circulation, ecosystems, and biogeochemical cycling simulated for a business-as-usual CO_2 emission scenario until year 4000 AD, *Global Biogeochem. Cycles*, *22*, GB1013, doi:10.1029/2007GB002953.

Sigman, D. M., M. A. Altabet, R. Michener, D. C. McCorkle, B. Fry, and R. M. Holmes (1997), Natural abundance-level measurment of the nitrogen isotopic composition of oceanic nitrate: An adaptation of the ammonia diffusion method, *Mar. Chem.*, *57*(3–4), 227–242, doi:10.1016/S0304-4203(97)00009-1.

Sigman, D. M., M. A. Altabet, D. C. McCorkle, R. Francois, and G. Fischer (1999), The $\delta^{15}N$ of nitrate in the Southern Ocean: Consumption of nitrate in surface waters, *Global Biogeochem. Cycles*, *13*(4), 1149–1166, doi:10.1029/1999GB900038.

Sigman, D. M., R. Robinson, A. N. Knapp, A. van Green, D. C. McCorkle, J. A. Brandes, and R. C. Thunell (2003), Distinguishing between water column and sedimentary denitrification in the Santa Barbara Basin using the stable isotopes of nitrate, *Geochem. Geophys. Geosyst.*, *4*(5), 1040, doi:10.1029/2002GC000384.

Sigman, D. M., J. Granger, P. J. DiFiore, M. F. Lehmann, R. Ho, G. Cane, and A. van Green (2005), Coupled nitrogen and oxygen isotope measurements of nitrate along the eastern North Pacific margin, *Global Biogeochem. Cycles*, *19*, GB4022, doi:10.1029/2005GB002458.

Simmons, H. L., S. R. Jayne, L. C. S. Laurent, and A. J. Weaver (2004), Tidally driven mixing in a numerical model of the ocean general circulation, *Ocean Modell.*, *6*(3–4), 245–263, doi:10.1016/S1463-5003(03)00011-8.

Somes, C. J., A. Schmittner, and M. A. Altabet (2010), Nitrogen isotope simulations reveal the importance of atmospheric iron deposition on N_2 fixation across the Pacific, *Geophys. Res. Lett.*, doi:10.1029/2010GL044537, in press.

Thamdrup, B., and T. Dalsgaard (2002), Production of N_2 through anaerobic ammonium oxidation coupled to nitrate reduction in marine sediments, *Appl. Environ. Microbiol.*, *68*(3), 1312–1318, doi:10.1128/AEM.68.3.1312-1318.2002.

Tyrrell, T. (1999), The relative influences of nitrogen and phosphorus on oceanic primary production, *Nature*, *400*, 525–531, doi:10.1038/22941.

Voss, M., J. W. Dippner, and J. P. Montoya (2001), Nitrogen isotope patterns in the oxygen-deficient waters of the eastern tropical North Pacific, *Deep Sea Res., Part I*, *48*(8), 1905–1921, doi:10.1016/S0967-0637(00)00110-2.

Wada, E. (1980), Nitrogen isotope fractionation and its significance in biogeochemical processes occurring in marine environments, in *Isotope Marine Chemistry*, edited by E. D. Goldberg et al., pp. 375–398, Uchida-Rokakuho, Tokyo.

Wada, E., and A. Hattori (1978), Nitrogen isotope effects in the assimilation of inorganic nitrogenous compounds by marine diatoms, *Geomicrobiology J.*, *1*(1), 85–101, doi:10.1080/01490457809377725.

Waser, N. A. D., P. J. Harrison, B. Nielsen, S. E. Calvert, and D. H. Turpin (1998), Nitrogen isotope fractionation during the uptake and assimilation of nitrate, nitrite, ammonium, and urea by a marine diatom, *Limnol. Oceanogr.*, *43*(2), 215–224, doi:10.4319/lo.1998.43.2.0215.

Weaver, A. J., et al. (2001), The UVic Earth system climate model: Model description, climatology, and applications to past, present and future climates, *Atmos. Ocean*, *39*(4), 361–428.

White, A. E., Y. H. Spitz, and D. M. Karl (2006), Flexible elemental stoichiometry in Trichodesmium spp. and its ecological implications, *Limnol. Oceanogr.*, *51*(4), 1777–1790.

Wu, J., W. Sunda, E. A. Boyle, and D. M. Karl (2000), Phosphate depletion in the western North Atlantic Ocean, *Science*, *289*, 759–762, doi:10.1126/science.289.5480.759.

Zehr, J. P., J. B. Waterbury, P. J. Turner, J. P. Montoya, E. Omoregie, G. F. Steward, A. Hansen, and D. M. Karl (2001), Unicellular cyanobacteria fix N_2 in the subtropical North Pacific Ocean, *Nature*, *412*, 635–638, doi:10.1038/35088063.

M. A. Altabet, School for Marine Science and Technology, University of Massachusetts Dartmouth, North Dartmouth, MA 02747, USA.

A. Bourbonnais and M. Eby, School of Earth and Ocean Sciences, University of Victoria, Victoria, BC V8W 2Y2, Canada.

E. D. Galbraith, Department of Earth and Planetary Science, McGill University, Montreal, QC H3A 2T5, Canada.

M. F. Lehmann, Institute for Environmental Geoscience, University of Basel, CH-4003 Basel, Switzerland.

R. M. Letelier, A. C. Mix, A. Schmittner, and C. J. Somes, College of Oceanic and Atmospheric Sciences, Oregon State University, Corvallis, OR 97331, USA. (csomes@coas.oregonstate.edu)

J. P. Montoya, School of Biology, Georgia Institute of Technology, Atlanta, GA 30332, USA.